Processing and Application of Ceramics 12 [4] (2018) 326–334
https://doi.org/10.2298/PAC1804326O

Preparation of TiO_2 and ZnO dispersions for inkjet printing of flexible sensing devices

Nejra Omerović[1,*], Marko Radović[1], Slavica M. Savić[1], Jaroslav Katona[2]

[1]*University of Novi Sad, BioSense Institute, Nano and Microelectronics Group, Dr Zorana Đinđića 1, 21000 Novi Sad, Serbia*
[2]*University of Novi Sad, Faculty of Technology Novi Sad, Bulevar cara Lazara 1, 21000 Novi Sad, Serbia*

Received 29 June 2018; Received in revised form 30 September 2018; Accepted 29 October 2018

Abstract

Research presented in this article focuses on the preparation of functional dispersions for inkjet printing of nanoparticles as sensitive layers. The stable suspensions of MO_x (M = Ti, Zn) were prepared using gum arabic (GA) and Solsperse® 40000 (SO) as dispersants. A special attention was paid to the monitoring of particle size evolution during the planetary ball milling of dispersions, so that optimum ratio between milling time and particle size can be determined. After adjusting the printing parameters, prepared inks were printed on the flexible PET substrate with interdigitated electrodes (IDE). Films printed with TiO_2 ink stabilized by GA exhibited highly cracked surface which resulted in low current values, whereas ZnO ink stabilized by SO yielded crack-free surface and much higher current values. All investigated samples showed linear current behaviour in the range from -5 to 5 V, indicating formation of ohmic contacts between electrodes and nanoparticles, but ZnO ink produced the highest current values. Gas sensing properties, tested at room temperature at several humidity levels and for different types of alcohols, revealed that printed sensor exhibits modest sensitivity for low humidity levels and slightly higher affinity towards methanol gas. Photo sensitivity measurement showed very high photocurrent values with strong potential for optoelectronic applications.

Keywords: *ZnO, TiO_2, inkjet printing, sensors*

I. Introduction

Although the most common use of the inkjet printing is in conventional applications such as graphics, text printing or marking, over the last decades the technology has been guided to manufacture novel functional surfaces and components with applications for advanced technologies. This is due to the ability of the inkjet printing to digitally control the ejection of ink droplets of defined volume and precisely position them onto a substrate [1–3]. Inkjet printing is a contactless process which means that wide range of fluids can be used and optimized for a variety of substrates, even non-flat, rigid or flexible ones. Besides this flexibility, short production time, low-cost and very efficient use of materials can be listed as main advantages of the inkjet printing [2–5].

Inkjet printing is one of the most versatile tools for functionalization of MO_x (metal oxides) nanomaterials into electronic components and devices [6]. Due to their unique structure, morphology, chemical, optical and electrical properties, MO_x nanomaterials have wide scope of applications in advanced technologies. Using suitable dispersions, these nanomaterials are printed as components for solar cells [7,8], photodetectors [9], gas sensors [10] and biosensors [11,12]. Cost-effective solutions to ambient monitoring, based on printed MO_x nanomaterials, have strong impact on modern food production industry, which is today the fastest growing market for inkjet printing technology. Food decay process is often followed by the emission of volatile organic compounds (VOC) like alcohols [13], therefore a lot of attention is focused on the development of highly efficient sensors, operating at room temperature and having high sensitivity [14]. Smart packaging technology often requires sensor operation at different humidity levels, ranging from low to high, for mushrooms, maize, grains, spices and tomatoes [15]. Significant efforts have

* Corresponding authors: tel: +381 21 485 2138,
e-mail: *nejra@biosense.rs*

been devoted to the optimization of breathalyser devices for monitoring concentration of ethanol vapour in human breath [16]. One of the advantages for application of the inkjet technology in diagnostic devices is the ability to rapidly produce low cost solutions printed on common paper substrate [17]. All these challenges have spanned together chemistry, physics, material science, biology and engineering in a joint multidisciplinary research of sensor design and applications. The most important challenges for printing of MO_x nanomaterials are the preservation of the material fundamental properties trough the printing process and providing conditions for maximum efficiency of the materials performance.

The aim of this work was to demonstrate the possibility of the inkjet printing of stable homogeneous aqueous suspensions of MO_x onto flexible, environmentally friendly, low-cost substrates addressing the requirements of flexible electronics for a cost-efficient, high-output manufacturing and opening the route towards the flexible, eco-designed mass production. The investigations on the optimum concentration of dispersants and the mechanism determining the dispersion behaviour of MO_x in aqueous dispersants solution were performed. The main goal of this work is to analyse the influences of different quantity of dispersants and milling conditions on the printing quality parameters of the ink using different substrates.

II. Experimental procedure

Fabrication of basic components of sensor devices such as transducer and sensitive layer was performed with simple and cost-effective inkjet printing technique. A schematic representation of sensor fabrication with inkjet technology is shown in Fig. 1. Transducer used in this work is composed of IDE printed with commercial Ag ink on flexible substrate. The sensitive layer with MO_x nanoparticles is printed as rectangular film on top of the electrodes. Utilization of the inkjet printing offers very precise patterning on various types of substrates with efficient use of nanomaterials and also provides substantial operating flexibility since it does not require the use of masks and other complicated processing steps.

For the preparation of functional inks we have used commercially available titanium oxide (TiO_2, anatase, 99.7%, Sigma Aldrich, US) and zinc oxide (ZnO, 99+%, Alfa Aesar, US) nanopowders. For the matrix preparation we have used gum arabic (GA, polyanionic hydrocolloide, Sigma Aldrich, US), *Solsperse*® 40000 (SO, anionic phosphate alkoxylated polymer, Lubrizol, US); *Byk*®-028 (antifoaming agent, BYK Additives & Instruments, Germany); 1,2-propylene glycol ($C_3H_8O_2$, Centrohem, Serbia), n-propanol (C_3H_8O, Kemika, Croatia). Printing of the interdigitated electrodes was performed using the Ag nanoparticle ink *SunTronic*® *Jet Silver* (SunChemical, UK).

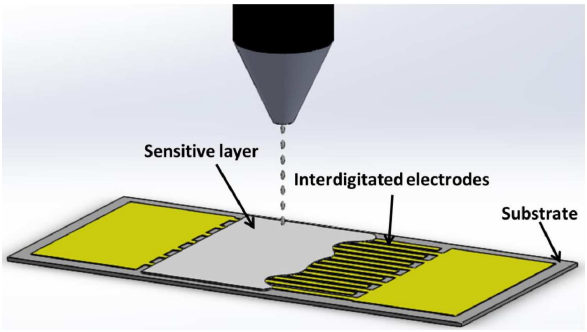

Figure 1. A schematic representation of fabricated sensor

The dispersions were homogenized by means of Ultraturrax T-25 homogenizer (IKA, Germany). The ball milling was performed using planetary ball mill PM 100 (Retsch, Germany) with YSZ (yttrium stabilized zirconia) 50 ml jar and balls of 2 mm in diameter. The viscosity of prepared inks was determined with RheoStress 600HP rheometer (Thermo Haake, Germany). Surface tension was measured with Sigma 703D tensiometer (KSV Instruments, Finland). Particle size determination was performed with Zetasizer Nano ZS (Malvern Instruments Ltd, UK), which works on the dynamic light scattering principle. Printing of the prepared inks was performed with Fuji Dimatix DMP-3000 (Fujifilm, Japan) semi-industrial inkjet printer. The optical images were collected using Huvitz HRM-300 optical microscope (Huvitz, South Korea). Atomic force microscopy (AFM) measurements were performed on NTEGRA prima (NDMT, Russia) microscope in semi-contact mode. The characterization of DC electrical properties was done on Yokogawa-Hewlett-Packard 4145A semiconductor analyser (Yokogawa Electronic, Japan). Humidity sensing characterization was performed using appropriate setup. Gas sensing properties of different alcohols (methanol, ethanol and propanol) were investigated using custom-built setup consisting of the chamber with mounted gas inlet/outlet for N_2 purging and equipped with fan and evaporator. Photocurrent measurements were made in the custom built setup equipped with high power light emitting diode operating at 365 nm.

III. Results and discussion

Design and optimization of functional inks, that can be used for inkjet printing of nanomaterials, can be considered as a bottom-up approach to achieve higher technological level, with the strong impact on the application of these materials in advanced technologies. Undertaken approach to the preparation of functional ink can be divided into 3 simple steps as shown in Fig. 2.

The primary dispersions of MO_x were prepared by dispersing either TiO_2 or ZnO nanopowder in a continuous phase. As the continuous phase, aqueous solution

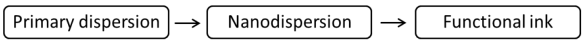

Figure 2. Basic steps used for preparation of functional ink for inkjet printing of TiO_2 and ZnO nanoparticles

Table 1. Chemical compositions of TiO_2 primary dispersions

Dispersion	TiO_2 [wt.%]	GA [wt.%]	SO [wt.%]	*Byk*® [wt.%]	H_2O [wt.%]	TiO_2 in H_2O [wt.%]	Dispersant in H_2O [wt.%]	TiO_2 : dispersant ratio
GATO-1	14.71	14.71			70.58	17.24	17.24	1 : 1
GATO-3.6	15.24	4.23		0.08	80.44	15.93	5.00	3.6 : 1
GATO-2.25	15.92	7.07		0.09	76.92	17.15	8.42	2.25 : 1
SOTO-45.2	15.82		0.35	0.35	83.48	15.93	0.42	45.2 : 1
SOTO-12.5	15.67		1.25	0.37	82.71	15.93	1.49	12.5 : 1

Table 2. Chemical compositions of ZnO primary dispersions

Dispersion	ZnO [wt.%]	GA [wt.%]	SO [wt.%]	*Byk*® [wt.%]	H_2O [wt.%]	ZnO in H_2O [wt.%]	Dispersant in H_2O [wt.%]	ZnO : dispersant ratio
GAZO-1	14.68	14.68		0.12	70.53	17.22	17.22	1 : 1
GAZO-3.6	15.25	4.24		0.04	80.47	15.93	5.00	3.6 : 1
SOZO-38.6	15.82		0.41	0.26	83.51	15.93	0.48	38.6 : 1

of dispersant GA or SO, in appropriate concentration, was used. The appearance of foam during homogenization imposed addition of suitable weight of antifoaming agent Byk®-028 in the continuous phase. The dispersions were homogenized by means of Ultraturrax T-25 homogenizer during 10 min at 15000 rpm and room temperature. The obtained dispersions with corresponding ratios are denoted as GATO (in the case of GA and TiO_2), SOTO (SO and TiO2), GAZO (GA and ZnO) and SOZO (SO and ZnO). The compositions of TiO_2 and ZnO primary dispersions are shown in Tables 1 and 2, respectively.

It is important to mention that for the preparation of dispersions with acceptable particle size and stability, the required concentration of SO is much lower compared to GA concentration, because of different structures and stabilization mechanisms of dispersants.

The primary dispersions, immediately after preparation, were further homogenized in planetary ball mill. The ball milling was performed using YSZ (yttrium stabilized zirconia) 50 ml jar and YSZ balls of 2 mm in diameter. For milling, 16.5 ml of primary dispersion was used. The milling conditions for prepared dispersions are shown in Table 3. TiO_2 and ZnO dispersions with higher concentration of GA in the formulation (GATO-1 and GAZO-1) were milled at 250 rpm for 180 min, and the particle sizes were simultaneously measured after 15, 30, 60, 90, 120, 150 and 180 min, in order to determine an optimum milling time.

Table 3. The milling conditions for TiO_2 and ZnO dispersions

Dispersion		Milling speed [rpm]	Milling time [min]
TiO_2	GATO-1	250	180
	GATO-3.6	250	90
	GATO-2.25	250 + 350	90 + 90
	SOTO-45.2	250	180
	SOTO-12.5	250	90
ZnO	GAZO-1	250	180
	GAZO-3.6	250	90
	SOZO-38.6	250	90

The primary dispersions, with GA as a dispersant, were prepared with the GA : TiO_2 and GA : ZnO ratio 1 : 1 and treated in planetary ball mill at 250 rpm for 180 min. Evolution of average particle size as a function of milling time is presented in Fig. 3. The milling of dispersions up to 90 min resulted in the significant reduction of the average particle size, which was the main goal of using planetary ball mill for the preparation of functional inks. For TiO_2 dispersion (GATO-1) the average particle size is reduced from 600 nm at the beginning to 420 nm after 90 min of milling, while in the case of ZnO dispersion (GAZO-1) the average particle size is reduced from 460 nm at the beginning to 330 nm after 90 min of milling. Prolonged milling time up to 180 min resulted in negligible changes of the average particle size for both dispersions. Therefore, milling time of 90 min can be considered as an optimal compromise between invested energy and achieved particle size.

Very important issue that needs to be addressed is the long term stability of the prepared dispersions. The particle size measurements during three weeks after preparation of dispersion, served as an indicator of colloidal

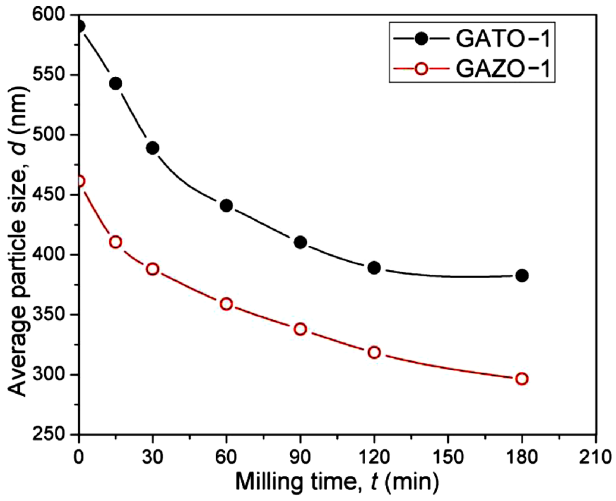

Figure 3. Variation in average particle size with milling time for GATO-1 and GAZO-1 primary dispersions

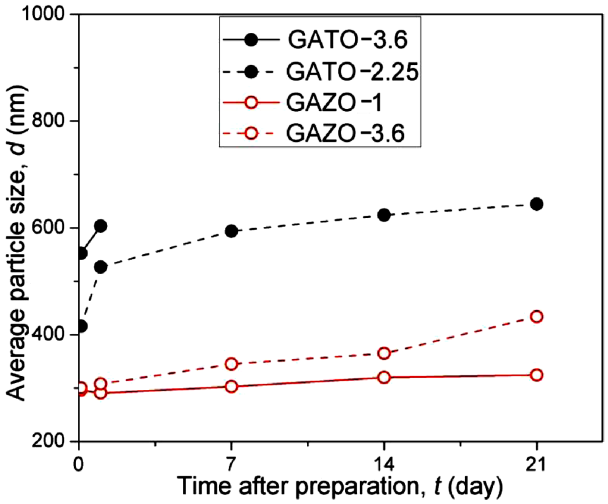

Figure 4. The average particle size of TiO_2 and ZnO primary dispersions stabilized with GA

stability. The dispersions GATO-1 and GAZO-1 showed good stability within the three weeks, but these dispersions were not used for functional inks preparation due to the high concentration of gum arabic, which is expected to have a strong influence on the properties of printed structures. Therefore, TiO_2 and ZnO primary dispersions with lower GA concentration (GATO-3.6 and GAZO-3.6) were prepared by milling at 250 rpm for 90 min. The average particle sizes, measured for TiO_2 and ZnO primary dispersions stabilized with GA, are displayed in Fig. 4. As can be seen (Fig. 4) the average particle size in TiO_2 dispersion GATO-3.6, after milling for 90 min is around 550 nm which means that the particle size is not decreased to the expected value. On the other hand, the average particle size in ZnO dispersion GAZO-3.6, after milling for 90 min, is around 300 nm, which is close to the achieved particle size in dispersion GAZO-1 after the same milling time.

It can also be seen (Fig. 4) that the average particle size of GATO-3.6 dispersion has increased for 10%, up to around 600 nm after one day, which indicated very unstable dispersion, while the average particle size of GAZO-3.6 dispersion stayed almost unchanged. During the third week, the average particle size of GAZO-3.6 was increased for 44%, up to around 430 nm. Although the new dispersion GAZO-3.6 displayed slightly worse stability compared to dispersion GAZO-1, due to the lower concentration of used dispersant, the GAZO-3.6 dispersion was used for functional ink preparation. In order to obtain more stable TiO_2 dispersion with smaller average particle size, the new dispersion GATO-2.25 was prepared. The dispersion GATO-2.25 was milled 180 min in total (90 min at 250 rpm + 90 min at 350 rpm). As can be seen in Fig. 4, smaller particles of TiO_2 dispersion were obtained with optimized milling conditions. The average particle size of the GATO-2.25 dispersion after 180 min of milling is around 400 nm. Although the GATO-2.25 dispersion, similarly as the GATO-3.6 dispersion, shows instability in the first 24 h after milling, it was used for functional ink formulation because of the smaller average particle size.

In order to examine how to prepare stable nanodispersions with SO as dispersant, two TiO_2 primary dispersions (SOTO-45.2 and SOTO-12.5) and one ZnO primary dispersion (SOZO-38.6) were prepared. The obtained results of the particle size measurements for TiO_2 and ZnO primary dispersions stabilized with SO are shown in Fig. 5. As can be seen, the dispersion SOZO-38.6 displayed good stability for the first two weeks, and a more significant increase in the particle size during the third week, up to around 350 nm, which is around 35% of the value obtained immediately after milling. The average particle size of the SOTO-12.5 dispersion is higher than that of the SOTO-45.2 dispersion, but dispersion SOTO-12.5 showed better stability during the time. The dispersions SOTO-12.5 and SOZO-38.6 were used for functional ink preparation.

Finally, two TiO_2 dispersions (GATO-2.25 and SOTO-12.5) and two ZnO dispersions (GAZO-3.6 and SOZO-38.6) were selected for functional ink preparation. Thus, four inkjet inks were prepared: two inks with TiO_2 nanoparticles (IJ-GATO-2.25 and IJ-SOTO-12.5) and two inks with ZnO nanoparticles (IJ-GAZO-3.6 and IJ-SOZO-38.6) according to the formulations from Table 4. The functional inks were prepared by diluting stable TiO_2 and ZnO nanodispersions with water and adding 1,2-propylene glycol (PG) and n-propanol (PrOH) in ratio PG : PrOH = 43 : 7. The water, PG and PrOH ratio in the formulations was H_2O : PG : PrOH = 50 : 43 : 7 which gives required values of viscosity and surface tension (η = 6.40 mPa s and σ = 36.20 mN/m) for printing. The formulations of the prepared inkjet inks are shown in Table 4.

The weight of PG-PrOH mixture, equal to the total weight of water in the formulation, was added to the previously diluted nanodispersion. Finally, inks were homogenized during 5 min at 15000 rpm and room tem-

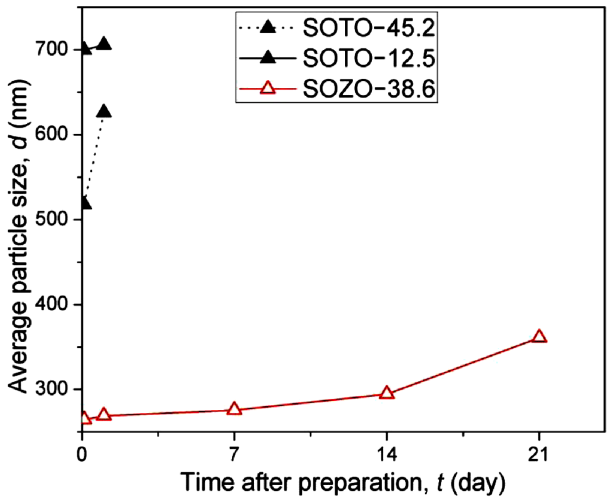

Figure 5. The average particle size of TiO_2 and ZnO primary dispersions stabilized with SO

Table 4. The formulations of inks used for inkjet printing of nanoparticles

Ink	MO_x [wt.%]	GA [wt.%]	SO [wt.%]	*Byk*® [wt.%]	PG [wt.%]	PrOH [wt.%]	H_2O [wt.%]	MO_x : dispersant ratio
TiO_2 – IJ-GATO-2.25	4.81	2.14		0.03	40	6.51	46.51	2.25 : 1
TiO_2 – IJ-SOTO-12.5	4.50		0.40	0.10	40.85	6.67	47.52	12.5 : 1
ZnO – IJ-GAZO-3.6	4.45	1.24		0.01	40.54	6.60	47.14	3.6 : 1
ZnO – IJ-SOZO-38.6	4.51		0.12	0.07	40.96	6.69	47.65	38.6 : 1

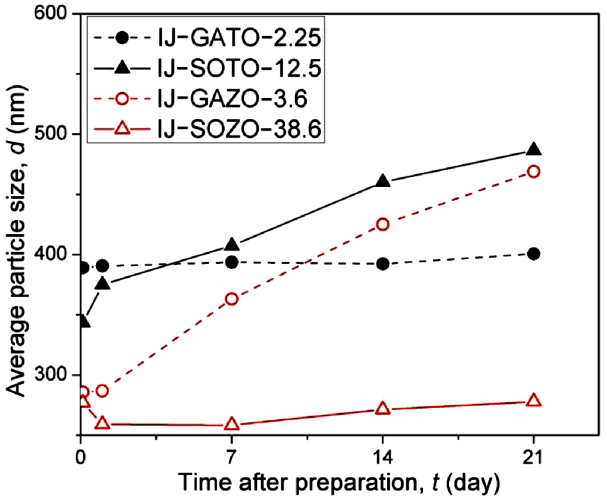

Figure 6. Stability test of the prepared inks, presented as variation in particle size during three weeks after preparation

perature by Ultraturrax T-25 homogenizer. The stability test of the prepared inks was conducted by measuring particle size during three weeks after preparation and the results are shown in Fig. 6. Negligible changes in particle size for inks IJ-GATO-2.25 and IJ-SOZO-38.6 can be observed, indicating good stability of these inks.

Based on the performed particle size measurements it can be concluded that the inks IJ-GATO-2.25 and IJ-SOZO-38.6 showed the best stability. In order to remove large particle aggregates and to reduce the risk of printhead nozzle clogging, prepared inks were filtered through 1 μm syringe filter (Whatman, UK) and loaded in the cartridge reservoir.

After successful preparation of inks, next step in the research was to optimize the printing parameters aiming to obtain a controllable and effective process for printing of nanoparticles that can be used for fabrication of sensitive sensor layers. By adjusting basic parameters of piezoelectric inkjet printer, such as jetting voltage, frequency and waveform, stable ink droplets, with an appropriate drop speed at 0.5 mm distance from the nozzle plate, were obtained. All prepared inks were printable and able to form stable droplets during jetting, except the TiO_2 ink stabilized with SO (IJ-SOTO-12.5), which showed the worst stability test after 3 weeks of aging.

Dropwatcher images of the IJ-SOZO-38.6 ink droplets ejection from the nozzles of printhead are shown in Fig. 7. It can be seen that after the drop leaves the nozzle it has a ligament, called tail, which ideally merges into the main drop without creating satellites (formation of satellites usually leads to the reduction in print quality).

In order to obtain continuous and homogeneous layer during inkjet printing, it was necessary to determine the optimal drop spacing by studying the behaviour of the printed ink drops on the substrate surfaces. An array of single ink drops on Si, polyimide (Kapton®), PET and paper substrates was printed at a mutual distance of 100 μm as shown in Fig. 8. The measured average drop diameter is 34 μm for Si, 32 μm for Kapton® and 40 μm for PET substrate. It must be noted that no coffee ring effect (a pattern left by a puddle of particle-laden liquid after it evaporates) was observed for all investigated substrates, since the appearance of this feature can lead to the degradation of the print quality. The printing of uniform layer on Si and Kapton® surfaces resulted in a formation of irregular structures due to the hydrophobic nature of these surfaces. For printing of sensitive layer of MO_x nanoparticles we have chosen PET substrate because it is hydrophilic and can be heated up to 200 °C. Taking into account the measured average drop diameter on the PET substrate, drop spacing which is half of the droplet size (20 μm) was used as the optimal value, aiming to create sufficient overlapping between individual droplets so that continuous layers can be printed.

The fabrication of the sensor transducer was performed by printing interdigitated electrodes (IDE) on flexible PET substrate, using commercial silver ink. The

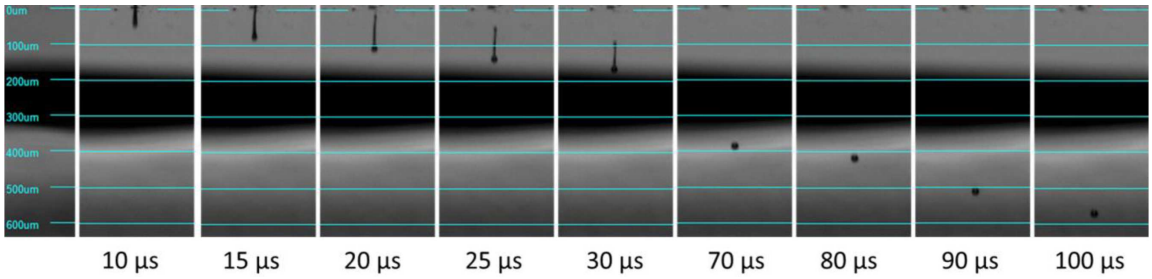

Figure 7. Dropwatcher images of the IJ-SOZO-38.6 ink droplets ejection from the nozzles of piezoelectric inkjet printhead

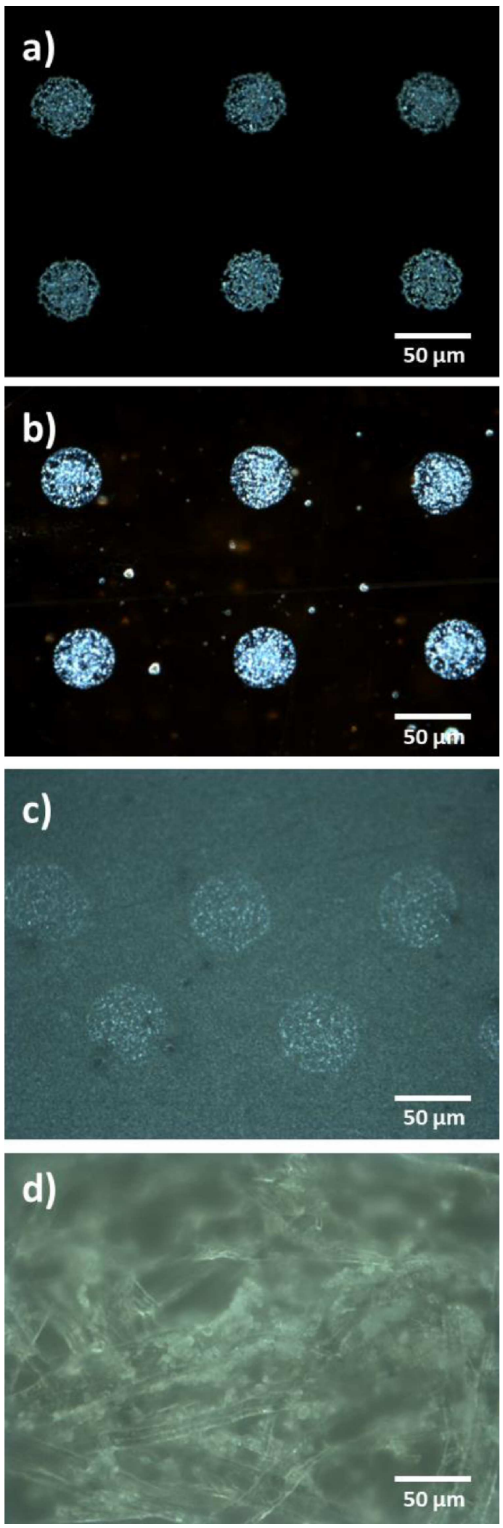

Figure 8. Optical images of individual drops of IJ-SOZO-38.6 ink printed on: a) Si, b) Kapton®, c) PET and d) paper substrate

optical image of the printed electrodes is given in Fig. 9. During the printing of the silver ink, the substrate was heated up at 40 °C, a step necessary for achievement of precisely resolved structures for electrical characterization. After printing, the IDE were gradually heated up to 200 °C and kept for 1 h to attain sintered Ag nanoparticles. The distance between fingers of IDE structure,

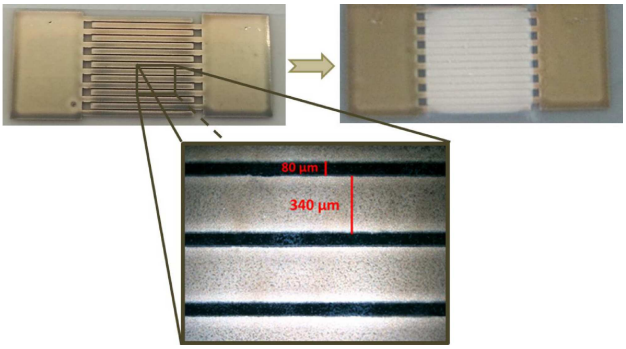

Figure 9. Optical images of IDE printed with Ag ink, along with image of the sensitive layer printed with IJ-SOZO-38.6 ink

after sintering, was around 80 µm, whereas the width of the individual finger was around 340 µm. PET substrate was chosen since it can withstand temperatures up to 200 °C allowing the sintering of printed electronic components and because of its flexibility, biodegradability and availability. In the second step rectangular layers of functional TiO_2 and ZnO inks were printed on top of the electrodes and they represent a sensitive sensor layer. By printing, a layer of liquid ink on the substrate was obtained, which was transformed into functional electronic element by evaporating volatile components of dispersion. After printing, the obtained sensors with rectangular (5 × 5 mm) sensitive layer were gradually heated up at 100 °C and kept at that temperature for 2 h to achieve evaporation of organic additives.

The successful preparation of inks with nanoparticles and optimization of printing parameters enabled printing of multilayer MO_x structures for sensing applications. Optical images of films printed with 10 layers using IJ-SOZO-38.6 and IJ-GATO-2.25 inks, together with corresponding AFM images of the printed nanoparticles are shown in Fig. 10. From the presented

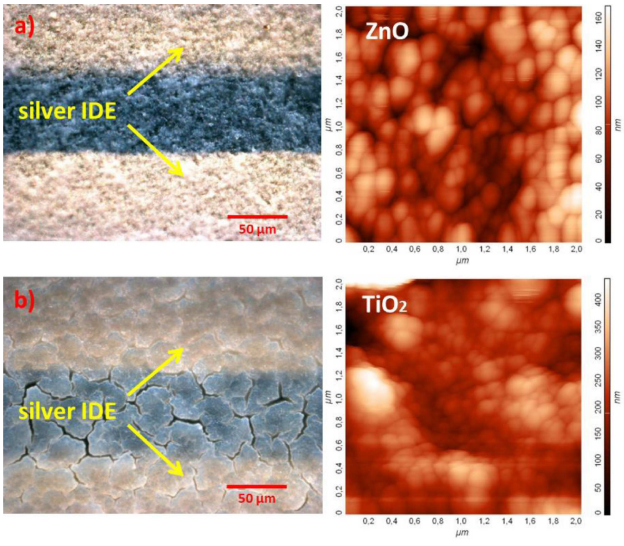

Figure 10. Optical images of films printed with 10 layers on top of IDE, using: a) IJ-SOZO-38.6 and b) IJ-GATO-2.25 inks, along with corresponding AFM images of printed ZnO and TiO_2 nanoparticles

optical images it can be clearly seen that ZnO ink (IJ-SOZO-38.6) produces consistent and homogeneous layer without cracks. The layer printed with TiO_2 ink (IJ-GATO-2.25) exhibits significant cracks on the surface of the film. The AFM images reveal nanostructured nature of printed films, where nanoparticles form large agglomerates. The agglomeration process is also observed during the preparation of the functional inks since the size of particles in primary dispersion is much larger than the initial size reported by manufacturers (TiO_2 APS < 25 nm; ZnO APS 40–100 nm). The particle size determined by the dynamic light scattering in primary dispersion is very similar to the size of agglomerates observed in AFM images, indicating that once the particles are stabilized in dispersion their size does not alter significantly during the inkjet printing process and after thermal treatment of the printed films.

The electrical characterization of the printed sensors was performed by measuring current vs. voltage ($I(V)$) curves in the -5 to 5 V range. In Fig. 11, $I(V)$ curves are compared for sensors printed with 10 layers of IJ-SOZO-38.6, IJ-GAZO-3.6 and IJ-GATO-2.25 inks. From the presented measurements it is evident that sensors printed with IJ-GAZO-3.6 and IJ-GATO-2.25 inks possess very high resistivity (very low current) which renders these samples not quite suitable for practical applications. Sensor printed with IJ-SOZO-38.6 ink exhibits significantly higher current values and linear voltage dependence pointing out that inkjet printed ZnO nanoparticles have ohmic contacts with silver electrodes. In the inset of Fig. 11 $I(V)$ curve for IJ-SOZO-38.6 ink without ZnO nanoparticles is shown, which displays essentially different behaviour compared to other presented results. The curve profile for the ink without nanoparticles presents clear evidence that the main contribution to the DC conductivity of printed film originates from ZnO nanoparticles. From the comparison of presented curves in Fig. 11, one can easily conclude that only sensor printed with IJ-SOZO-38.6 ink can be used for sensing purposes.

Transient response curves to different relative humidity levels, of the sensor printed with 10 layers of IJ-SOZO-38.6 ink are shown in Fig. 12. In the inset of Fig. 12 response/recovery curves are given for sensor response to different types of alcohol vapours with the same 50 ppm concentration. The performance of the printed sensor was tested at room temperature. Sensor response can be defined as [18]:

$$S = \frac{R_a}{R_g} \tag{1}$$

where R_a is sensor's resistivity in ambient gas and Rg is sensor's resistivity in the presence of target gas. From the dynamic response behaviour, presented in Fig. 12, it can be easily confirmed that for lower humidity levels sensor has relatively modest response, which is expected for ZnO nanoparticles [19]. For extremely high humidity conditions (RH = 90%) sensor response becomes drastic, most probably because of the several layers of physisorbed water on the surface of nanoparticles. For porous structures made of MO_x nanoparticles, in the low RH conditions where water molecules do not cover the reactive surface completely, dominant transport mechanism is based on the electronic conduction [20,21]. In the case of high relative humidity the physisorbed water covers the surface completely and the conduction mechanism is based on the proton transport between adjacent hydrogen sites. Such transport mechanism is independent of the properties of ZnO nanomaterial, so the sensor response becomes significantly higher as seen in Fig. 12.

Response/recovery time profiles of the same inkjet printed sensor to 50 ppm of methanol, propanol and ethanol vapours are shown in the inset of Fig. 12. Measurements are performed at RT and very low humid-

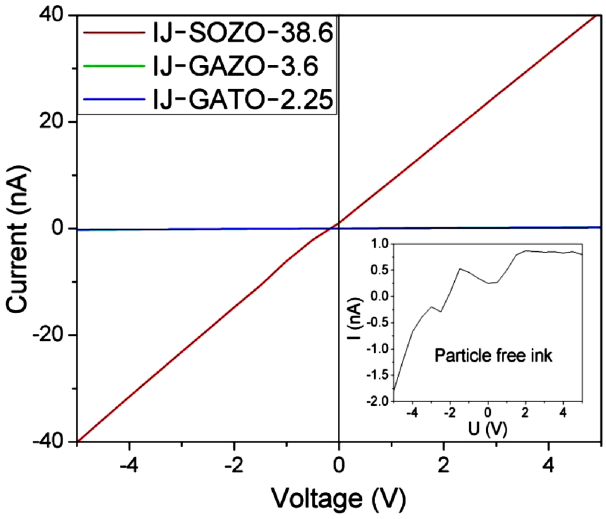

Figure 11. $I(V)$ curves for sensors printed with IJ-SOZO-38.6, IJ-GAZO-3.6 and IJ-GATO-2.25 inks (inset shows $I(V)$ curve for IJ-SOZO-38.6 ink without ZnO nanoparticles)

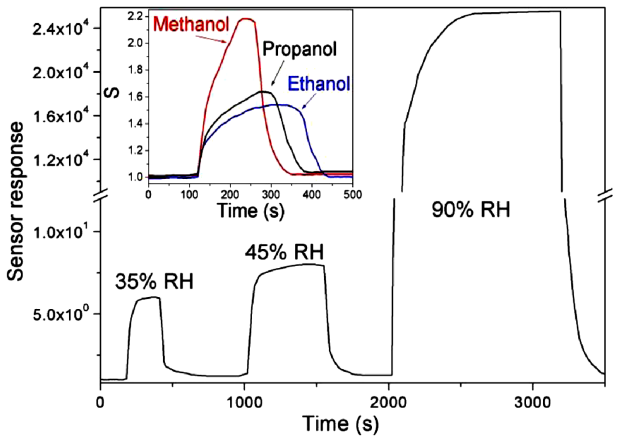

Figure 12. Transient response curves to different levels of relative humidity of the sensor printed with 10 layers of IJ-SOZO-38.6 ink (inset shows response/recovery time profiles of the sensor to 50 ppm ethanol, propanol and methanol vapour, measured at RT and 8% RH)

ity levels (8% *RH*) in order to determine true sensor response to alcohol vapours without interference of humidity. The target analyte concentration was set at 50 ppm, since it is typical concentration of alcohol vapour that can be detected during the food decay process [13], and tested with breath analyser [16]. Displayed responses reveal that printed SOZO sensor exhibits sensitivity to all tested alcohol vapours, and slight affinity to methanol gas. For methanol vapour sensor has the highest and the fastest response, whereas for propanol and ethanol vapour the response is lower with notably longer response and recovery times. By comparison of the gas sensitivity results we have concluded that designed sensors have good sensing characteristics, operating at room temperature, but the cross-sensitivity between the humidity and VOC vapours remains the big challenge for further optimization of this type of devices.

Inkjet printing of porous MO_x nanostructures can offer cutting-edge technology for photosensitive devices [9] and solar cells [7], due to their unique electronic structure and optical properties. The measurement of photocurrent for the sensor printed with 10 layers of IJ-SOZO-38.6 ink is given in Fig. 13. Light emitting diode (LED) operating at 365 nm with the power of 100 mW is used as excitation source. The wavelength of LED source is chosen to be in the visible spectral range and in the vicinity of the optical band gap of ZnO [22]. From the presented time-resolved response it can be seen that investigated sensor shows very high response to the incident light. By comparison with literature data for photocurrent values of ZnO based materials [23–25], one important fact can be established and that is very good photosensitivity with very high photocurrent values. These results offer great potential for application of the inkjet printed ZnO nanoparticles in solar cell devices where high photoconversion rates are required. It should be emphasized that rise and decay times (τ_r = 240 s; τ_d = 210 s) are longer than for previously published data [26], and these findings render sensor with ZnO nanoparticles not suitable for photosensitive devices, where fast response is required. Longer rise/decay times are probably the result of IDE configuration, and further optimization of the electrode design can lead to the improved photocurrent response.

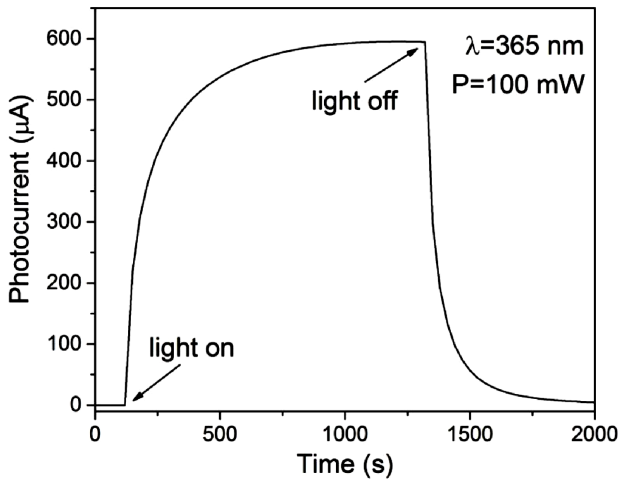

Figure 13. Photocurrent time resolved response of the sensor printed with 10 layers of IJ-SOZO-38.6 ink (excitation wavelength was 365 nm and LED power was set to 100 mW)

IV. Conclusions

A bottom-up approach to the inkjet fabrication of sensitive layers for sensing devices is demonstrated in this article. Main focus of the conducted research is optimization of functional dispersions for inkjet deposition of MO_x nanoparticles. PET substrate with Ag IDE was chosen as flexible transducer platform. On top of the electrodes multiple layers of prepared inks were printed in order to produce porous MO_x nanostructures for sensing applications. DC electrical transport characterization proved to be very useful for discrimination of the quality of the printed films since the IJ-GAZO-3.6 (gum arabic as dispersant and ZnO nanoparticles with ratio 1 : 3.6) and IJ-GATO-2.25 (gum arabic as dispersant and TiO_2 nanoparticles with ratio 1 : 2.25) inks showed much lower current values compared to the sensor printed with the IJ-SOZO-38.6 (*Solsperse*® 40000 as dispersant and ZnO nanoparticles with ratio 1 : 38.6) ink. Gas sensing measurements revealed that the sensor printed with the IJ-SOZO-38.6 ink had modest response to normal ambient humidity levels and very high response to extreme *RH* levels. The tested sensor had slight affinity to methanol vapour in comparison to propanol and ethanol at the 50 ppm concentration. The photocurrent measurements showed very good response to the excitation light with high photocurrent values, bringing strong impact on practical application of the inkjet printed flexible sensing devices.

Acknowledgement: This work was supported by the Serbian Ministry of Education, Science and Technological Development through projects III46010 and III44006.

References

1. B. Derby, "Inkjet printing ceramics: From drops to solid", *J. Eur. Ceram. Soc.*, **31** [14] (2011) 2543–2550.
2. J. Alamán, R. Alicante, J.I. Peña, C. Sánchez-Somolinos, "Inkjet printing of functional materials for optical and photonic applications", *Materials*, **9** [11] (2016) 910.
3. A. Friederich, J.R. Binder, W. Bauer, "Rheological control of the coffee stain effect for inkjet printing of ceramics", *J. Am. Ceram. Soc.*, **96** [7] (2013) 2093–2099.
4. B. Andò, S. Baglio, A.R. Bulsara, T. Emery, V. Marletta, A. Pistorio, "Low-cost inkjet printing technology for the rapid prototyping of transducers", *Sensors*, **17** [4] (2017) 748.
5. M. Rieu, M. Camara, G. Tournier, J.P. Viricelle, C. Pijolat, N.F. de Rooij, D. Briand, "Fully inkjet printed SnO_2 gas sensor on plastic substrate", *Sensors Actuators B*, **236** (2016) 1091–1097.

6. P. Calvert, "Inkjet printing for materials and devices", *Chem. Mater.*, **13** [10] (2001) 3299–3305.
7. Y. Oh, H.G. Yoon, S-N. Lee, H-K. Kim, J. Kim, "Inkjet-printing of TiO_2 co-solvent ink: From uniform ink-droplet to TiO_2 photoelectrode for dye-sensitized solar cells", *J. Electrochem. Soc.*, **159** [1] (2012) B34–B38.
8. A. Karpinski, S. Berson, H. Terrisse, M.M. Granvalet, S. Guillerez, L. Brohan, M. Richard-Plouet, "Anatase colloidal solutions suitable for inkjet printing: Enhancing lifetime of hybrid organic solar cells", *Solar Energy Mater. Solar Cells*, **116** (2013) 27–33.
9. B. Cook, Q. Liu, J. Butler, K. Smith, K. Shi, D. Ewing, M. Casper, A. Stramel, A. Elliot, J. Wu, "Heat-assisted inkjet printing of tungsten oxide for high-performance ultraviolet photodetectors", *ACS Appl. Mater. Interf.*, **10** [1] (2018) 873–879.
10. T. Järvinen, G.S. Lorite, A-R. Rautio, K.L. Juhász, Á. Kukovecz, Z. Kónya, K. Kordas, G. Toth, "Portable cyber-physical system for indoor and outdoor gas sensing", *Sensors Actuators B*, **252** (2017) 983–990.
11. A. Määttänen, U. Vanamo, P. Ihalainen, P. Pulkkinen, H. Tenhu, J. Bobacka, J. Peltonen, "A low-cost paper-based inkjet-printed platform for electrochemical analyses", *Sensors Actuators B*, **177** (2013) 153–162.
12. N. Komuro, S. Takaki, K. Suzuki, D. Citterio, "Inkjet printed (bio)chemical sensing devices", *Anal. Bioanal. Chem.*, **405** [17] (2013) 5785–5805.
13. D. Dong, C. Zhao, W. Zheng, W. Wang, X. Zhao, L. Jiao, "Analyzing strawberry spoilage via its volatile compounds using longpath Fourier transform infrared spectroscopy", *Sci. Reports*, **3** (2013) 2585.
14. D. Sebők, L. Janovák, D. Kovács, A. Sápi, D.G. Dobó, Á. Kukovecz, Z. Kónya, I. Dékány, "Room temperature ethanol sensor with sub-ppm detection limit: Improving the optical response by using mesoporous silica foam", *Sensors Actuators B*, **243** (2017) 1205–1213.
15. S. Yildirim, B. Röcker, M.K. Pettersen, J. Nilsen-Nygaard, Z. Ayhan, R. Rutkaite, T. Radusin, P. Suminska, B. Marcos, "Active packaging applications for food", *Compr. Rev. Food Sci. Food Safety*, **17** [1] (2018) 165–199.
16. M.A.G. Wallace, J.D. Pleil, "Evolution of clinical and environmental health applications of exhaled breath research: Review of methods and instrumentation for gas-phase, condensate, and aerosols", *Anal. Chim. Acta*, **1024** (2018) 18–38.
17. E. Bihar, Y. Deng, T. Miyake, M. Saadaoui, G.G. Malliaras, M. Rolandi, "A disposable paper breathalyzer with an alcohol sensing organic electrochemical transistor", *Sci. Reports*, **6** (2016) 27582.
18. L.-J. Bie, X.-N. Yan, J. Yin, Y.-Q. Duan, Z.-H. Yuan, "Nanopillar ZnO gas sensor for hydrogen and ethanol", *Sensors Actuators B*, **126** [2] (2007) 604–608.
19. G. Niarchos, G. Dubourg, G. Afroudakis, M. Georgopoulos, V. Tsouti, E. Makarona, V. Crnojevic-Bengin, C. Tsamis, "Humidity sensing properties of paper substrates and their passivation with ZnO nanoparticles for sensor applications", *Sensors*, **17** [3] (2017) 516.
20. Z. Wang, L. Shi, F. Wu, S. Yuan, Y. Zhao, M. Zhang, "The sol-gel template synthesis of porous TiO_2 for a high performance humidity sensor", *Nanotechnology*, **22** [27] (2011) 275502.
21. J. Bai, B. Zhou, "Titanium dioxide nanomaterials for sensor applications", *Chem. Rev.*, **114** [19] (2014) 10131–10176.
22. E.A. Meulenkamp, "Synthesis and growth of ZnO nanoparticles", *J. Phys. Chem. B*, **102** [29] (1998) 5566–5572.
23. D. Lin, H. Wu, W. Zhang, H. Li, W. Pan, "Enhanced UV photoresponse from heterostructured Ag-ZnO nanowires", *Appl. Phys. Lett.*, **94** (2009) 172103.
24. M. Furuta, Y. Kamada, M. Kimura, S. Shimakawa, T. Kawaharamura, D. Wang, C. Li, S. Fujita, T. Hirao, "Photocurrent and persistent photoconductivity in zinc oxide thin-film transistors under ultraviolet-light irradiation", *Jpn. J. Appl. Phys.*, **50** (2011) 110204.
25. F. Zahedi, R.S. Dariani, S.M. Rozeti, "Structural, optical and electrical properties of ZnO thin films prepared by spray pyrolysis: Effect of precursor concentration", *Bull. Mater. Sci.*, **37** [3] (2014) 433–439.
26. V.K. Dwivedi, P. Srivastava, G. Vijaya Prakash, "Photoconductivity and surface chemical analysis of ZnO thin films deposited by solution-processing techniques for nano and microstructure fabrication", *J. Semicond.*, **34** [3] (2013) 033001.